Effect of chain stiffness on ion distributions around a polyelectrolyte in multivalent salt solutions

Yu-Fu Wei and Pai-Yi Hsiao*

Department of Engineering and System Science,

National Tsing Hua University, Hsinchu, Taiwan 300, R.O.C.

(Dated: December 21, 2009)

Abstract

Ion distributions in dilute polyelectrolyte solutions are studied by means of Langevin dynamics simulations. We show that the distributions depend on the conformation of a chain while the conformation is determined by the chain stiffness and the salt concentration. We observe that the monovalent counterions originally condensed on a chain can be replaced by the multivalent ones dissociated from the added salt due to strong electrostatic interaction. These newly condensed ions give an important impact on the chain structure. At low and at high salt concentrations, the conformation of a semiflexible chain is rodlike. The ion distributions show similarity to those for a rigid chain, but difference to those for a flexible chain whose conformation is a coil. In the mid-salt region, the flexible chain and the semiflexible chain collapse but the collapsed chain structures are, respectively, disordered and ordered structures. The ion distributions hence show different profiles for these three chain stiffness with the curves for the semiflexible chain lying between those for the flexible and the rigid chains. The number of the condensed multivalent counterions, as well as the effective chain charge, also shows similar behavior, demonstrating a direct connection with the chain morphology. Moreover, we find that the condensed multivalent counterions form triplets with two adjacent monomers and are localized on the chain axis at intermediate salt concentration when the chain stiffness is semiflexible or rigid. The microscopic information obtained here provides valuable insight to the phenomena of DNA condensation and is very useful for researchers to develop new models.

PACS numbers:

*corresponding author; e-mail: pyhsiao@ess.nthu.edu.tw

I. INTRODUCTION

Polyelectrolytes (PEs), such as DNA molecules and many synthetic polymers, are macromolecules carrying a large number of charged groups which are ionizable in water. The presence of long-ranged electrostatic interaction and the confinement of charges on chains, together with the degree of freedom of chain conformation, make this kind of system very complicated and unpredictable. The behavior of PEs is greatly influenced by ions in the solutions, owing to the screening effect and ionic redistribution. For example, addition of salt in the solutions, especially multivalent salt, can change drastically the properties of PEs [1, 2, 3, 4, 5]. When salt is added, the multivalent counterions dissociated from the salt can compete with the monovalent ones in the solutions and condense onto PE chains, which eventually leads the system to a series of phase transition. The condensation of multivalent counterions is a process of both energetic and entropic favor because a Z-valent counterion ($Z > 1$) attracting to a PE chain is Z times stronger than a monovalent one and the release of Z monovalent counterions into the solution, due to the condensation of the Z-valent counterion, also increases the system entropy [6, 7, 8]. A phase separation takes place when salt concentration is higher than a critical value. The chains collapse and aggregate in the solution, resulting in a precipitation from the solution. When the salt concentration is further increased and goes beyond a second critical value, the precipitated PEs redissolve back into the solution. The system returns to a homogeneous phase [9, 10, 11]. The phase transition occurred at the first critical salt concentration is a result of ionic screening and bridging of multivalent counterions bound near PEs [3, 12, 13]. The transition occurred at the second one exists several explanations [2, 14, 15, 16, 17]. One of them attributes the resolubilization of PEs to the occurrence of charge inversion of PEs [17]. It argues that the condensed multivalent counterions can overcompensate the chain charge when salt concentration is high, and the repulsive force between chain segments due to the charge of inverted sign at that moment causes the segregation and resolubilization of chains. Another theory considers the Bjerrum association between ions [16]. By using a two-state model of chain, it predicts the possibility of either sign of the effective chain charge under different conditions. These theories usually over-simplifies the situations and are constructed based upon certain preassumed chain conformation and ion distribution. Further verification is thus needed. To understand the systems, it is important to study chain conformation and ion distributions

around a chain in solutions. We have investigated the first issue, the effect of chain stiffness on PE chain conformation, in our previous paper [43]. In this work, we focus on the second issue: the ion distribution.

To investigate ion distributions directly from experiments is difficult. Computer simulation, on the contrary, can do it easily because the positions of atoms are explicitely given in the study. This issue can be investigated on different scales [18, 19, 20, 21, 22, 23, 24, 25, 26, 27, 28, 29, 30, 31, 32]. An all-atom model, which simulates molecules with detailed chemical composition and structure, are usually applied in the study of small systems for short simulation time, owing to high computational cost related to today's computer power [18, 19, 20]. Space and time scales are both restricted. A coarse-grained model, which reduces the complexity of the molecular structure by grouping atoms, on the other hands, can decrease significantly the computational cost. Researchers can hence investigate larger systems evolving over a longer simulation time. Using coarse-grained models, scientists have investigated ion distribution and effective interaction and free energy of DNA molecule systems [21, 22, 23, 24]. The chains were modeled by an infinitively long post through periodic boundary condition. This model preserved the DNA helical structure and can be used to study local structural transitions, such as the B-to-Z transition, in addition to the ion distribution. However, it fails to characterize the global chain conformation, as what happened in DNA condensation when polyvalent ions are added into the solution.

To study the collapse and the reexpansion of single PE chains, bead-spring chain models are usually employed [25, 26, 27, 28, 29, 30, 31, 32]. This kind of simple models allows people to investigate the behavior of PE systems in a large space and time scale. By exploiting it, researchers have demonstrated that various conformational transitions of PE chains take places under different conditions. The models could be hence good candidates in the study of ion distribution related to the chain conformations. Liu and Muthukumar showed that a chain can be collapsed in a salt-free solution when Coulomb coupling strength is strong [25]. Their study reveals the relation between counterion condensation and the formation of local dipole moment. Hsiao and Luijten studied how PE chains are collapsed in multivalent salt solutions [33]. They found that the chains are charge overcompensated at their very surface when the amount of the multivalent counterions of salt is greater than the amount needed to neutralize the bare chain charge [33]. Counterion condensation on a PE chain has also been studied by several groups [25, 29, 34]. However, these studies aimed to understand the

collapse transition of chain happened in salt-free or low-salt conditions. The information concerning the unfolding transition of chain provoked by high concentration of counterions was missing. In this work, we plane to study the ion distribution around a PE chain in solutions over a wide range of salt concentration, so wide that single chains can subsequently undergo collapse and reexpansion transitions, using a bead-spring chain model. The focus will be the exploitation of the ion distribution at different salt concentrations and the relation with the chain conformation.

It is known that the structure of collapsed PE chains depends sensitively on the chain rigidity [35, 36, 37]. Studies also showed that the rigidity determines the transition of chain conformation to be continuous or discrete [38, 39, 40, 41, 42, 43]. It is, therefore, very relevant to know how ion distributions are influenced by the chain rigidity in the problem of PE condensation. Ou and Muthukumar observed that the number of the condensed monovalent counterions on a chain decreases in a salt-free solution when chain stiffness increases [27]. Sarraguça and Pais studied PE chains collapse by trivalent salt in different circumstances [29]. They found that the density of trivalent ions around stiff chains is smaller than around flexible ones. Moreover, flexible chains are compacted into smaller dimensions and the ion correlation is strong due to small volume of the confinement. Nonetheless, the situation for high salt concentrations where chain reexpansion occurs was not discussed.

This paper is organized as follows. We describe our model and the simulation setup in Section II. The results and discussions are given in Section III. After a short revisit of the dependence of chain size and morphology on the salt concentrations for flexible, semiflexible and rigid chains in Section III A, we investigate various ion distributions in PE solutions. The topics include the integrated ion distribution in the radial direction of a chain (Section III B), the charge distribution (Section III C), the ion condensation and the effective chain charge (Section III D), the condensed ion distribution along a chain backbone (Section III E), and the radial distribution functions (Section III F). By investigating these topics, we can make connection between ion distributions and chain conformations and understand the role of chain stiffness in different salt regions. Moreover, the results obtained from the rigid-chain case provide a direct verification of the Manning condensation theory by simulations. We give our conclusions in Section IV.

II. MODEL AND SETUP

Our system consists of a PE chain and tetravalent salt molecules, placed in a cubic box with periodic boundary condition. The chain dissociates into a polyion and many counterions. The polyion is modeled by a bead-spring chain and comprises 48 beads. Each bead carries a negative unit charge $-e$. The counterions are modeled by charged spheres, carrying a $+e$ charge each. The tetravalent salt dissociates into tetravalent cation (counterions) and monovalent anions (coions). These ions are also modeled by charged spheres. Solvent molecules are not explicitly incorporated in the study. Nonetheless, we consider the entire solvent as a dielectric medium with dielectric constant equal to ϵ_r.

We consider two kinds of non-bonded interactions: the excluded volume interaction and the Coulomb interaction, applied to all the beads on the chain and spheres in the system, and two kinds of bonded interactions: the connectivity and the chain rigidity, applied solely to the chain. The excluded volume is modeled by a purely repulsive Lennard-Jones (LJ) potential

$$U_{LJ}(r) = \begin{cases} 4\varepsilon_{LJ}\left[(\sigma/r)^{12} - (\sigma/r)^{6}\right] + \varepsilon_{LJ} & \text{for } r \leq 2^{1/6}\sigma \\ 0 & \text{for } r > 2^{1/6}\sigma \end{cases} \tag{1}$$

where r is the distance, ε_{LJ} is the interaction strength and σ represents the diameter of a particle. We assume identical ε_{LJ} and σ for the ion spheres and monomer beads. The Coulomb interaction between two charged ions or beads is given by

$$U_{coul}(r) = \frac{Z_i Z_j \lambda_B k_B T}{r} \tag{2}$$

where Z_i and Z_j are charge valences, k_B is the Boltzmann constant, T is the temperature, and $\lambda_B = e^2/(4\pi\epsilon_0\epsilon_r k_B T)$ is the Bjerrum length (ϵ_0 is the vacuum permittivity and ϵ_r the solvent dielectric constant). The connectivity of two consecutive beads on the chain is described by a finitely extensible nonlinear elastic potential

$$U_{sp}(b) = -\frac{1}{2} k_b b_{max}^2 \ln\left(1 - \frac{b^2}{b_{max}^2}\right) \tag{3}$$

where b is the length of a bond, b_{max} is the maximum bond extention, and k_b is the spring constant. The chain rigidity is represented by a harmonic angle potential,

$$U_{angle}(\theta) = k_a(\theta - \pi)^2 \tag{4}$$

where θ is the bond angle between two consecutive bonds and k_a is the force constant.

In addition to the above interactions, two more forces are exerted on each particle. They are (1) a dissipative force, which takes into account the friction force due to the particle moving through the solvent, and (2) a stochastic force, which models the thermal collisions by solvent molecules. The equation of motion, also known as the Langevin equation, reads as

$$m\ddot{\vec{r}}_i = -\frac{\partial U}{\partial \vec{r}_i} - m\gamma\dot{\vec{r}}_i + \vec{\eta}_i(t) \tag{5}$$

where m is the mass of particle, γ is the friction coefficient, and $\vec{\eta}_i$ is the stochastic force. We have assumed identical m and γ for all the particles. The system reaches an equilibrium state with the temperature given by the fluctuation-dissipation theorem:

$$\langle \vec{\eta}_i(t) \cdot \vec{\eta}_j(t') \rangle = 6k_B T m\gamma\delta_{ij}\delta(t-t') \tag{6}$$

where δ_{ij} and $\delta(t-t')$ are the Kronecker and the Dirac delta functions, respectively.

We set $\varepsilon_{LJ} = k_B T/1.2$, $k_b = 5.8333 k_B T/\sigma^2$, $b_{max} = 2\sigma$ and $\lambda_B = 3\sigma$. γ is set to $15\tau^{-1}$ (where $\tau = \sigma\sqrt{m/(k_B T)}$) to mimic aqueous solutions. These setups give a linear charge density of chain corresponding to a value typically for many polyelectrolyte systems, such as sodium polystyrene sulfonate. We varied k_a over a large range from 0 to $100 k_B T/rad^2$ to study the effect of chain stiffness. The values cover three typical chain stiffness: flexible chains, semiflexible chains, and rigid chains (see explanation in Section III A). The (4:1)-salt concentration C_s is varied from 0 to $0.01024\sigma^{-3}$ whereas the monomer concentration C_m is fixed at $3.2 \times 10^{-4}\sigma^{-3}$. The size of the simulation box is 53.13σ, which is large enough to avoid chain overlapping under periodic boundary condition. Therefore, the studied case is a dilute PE solution. It has been shown in experiments [10] and simulations [32] that PEs show similar condensation and decondensation behavior in the dilute region. The largest system in our study contains totally 7776 charged particles. We list all the values of C_s investigated and the corresponding numbers of tetravalent counterions and monovalent coions in Table I for reader's reference.

We perform Langevin dynamics simulations with the integrating time step equal to 0.005τ. The Coulomb interaction is calculated by the technique of Ewald sum. An equilibration phase takes about 10^7 time steps of run, followed by a production phase cumulating data for 10^7 to 3×10^8 time steps. In order to sample sufficiently the data, several independent runs are performed at each salt concentrations, starting with different initial configurations. To simplify the notation, in the rest of the text, length, energy, and time will be measured

C_s ($\times 10^{-5}$)	#(+4)-ions	#(−1)-ions
0.667	1	4
1.33	2	8
2.67	4	16
4.00	6	24
5.33	8	32
8.00	12	48
16.0	24	96
32.0	48	192
64.0	96	384
128	192	768
256	384	1536
512	768	3072
1024	1536	6144

TABLE I: Values of C_s and the corresponding numbers of tetravalent counterions and monovalent coions in the simulation box

in unit of σ, k_BT, and τ, respectively. Therefore, concentration will be described in unit of σ^{-3} and k_a in unit of k_BT/rad^2, and so on.

III. RESULT AND DISCUSSION

A. Chain size, morphology, and bond length

In this section, we shortly revisit some of the major findings obtained in our previous work [43], how the chain size and morphology depend on the chain stiffness in multivalent salt solutions, to give readers a thorough picture of the system. The detailed discussions can be found in the paper [43]. Starting from the next section, we will study ion distributions and show that they depend strongly on the size and the morphology of PE chains in solutions.

Instead by using the radius of gyration, we characterize here the chain size by the hydrodynamic radius, R_h, which is the Stokes radius of a polymer moving through a solution [44]. R_h is calculated by the equation $R_h^{-1} = (\Sigma_{i=1}^{N}\Sigma_{j=1,j\neq i}^{N} r_{ij}^{-1})/N^2$. The results, R_h vs. C_s, for

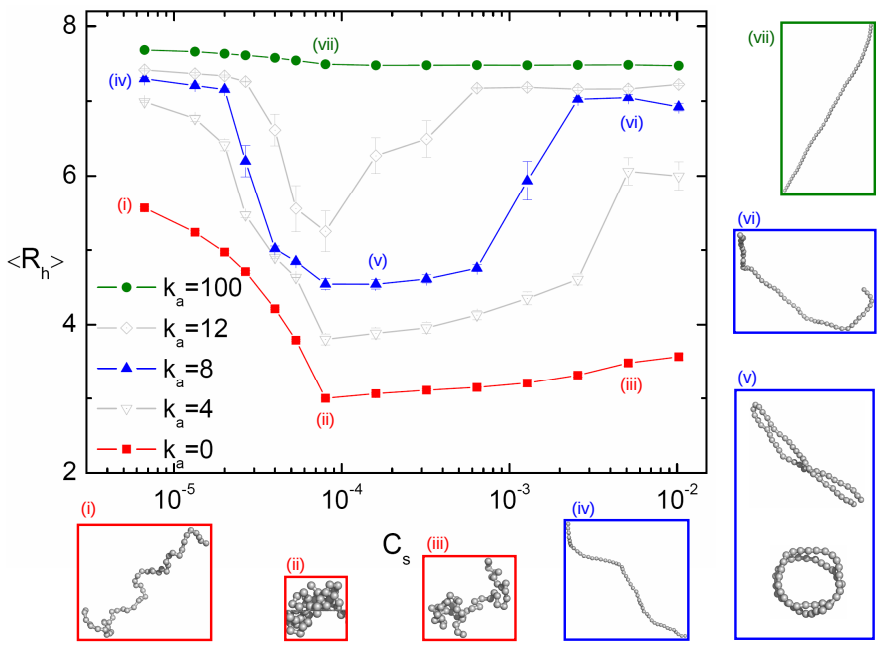

FIG. 1: Mean hydrodynamic radius $\langle R_h \rangle$ as a function of tetravalent salt concentration C_s. Snapshots of some typical chain structures at the points (i) to (vii) are shown by the side of the figure.

different chain stiffness k_a are presented in Fig. 1.

We can see that the curves show different variations against C_s, depending on the chain stiffness. These variations can be classified into three types. The first type is attributed to the case of small k_a such as $k_a = 0$. The chain is said *flexible* and R_h in the semi-log plot looks similar to a tilted-L curve. The second type is addressed to intermediate k_a, such as $k_a = 8$. The chain is called *semiflexible*, for which the R_h curve takes a shape similar to the letter 'U'. The third type is ascribed to large k_a like $k_a = 100$. The chain is very stiff and there is basically no variation against C_s; we are in the case of *rigid* chains.

Snapshots for these three types of variations are shown by the side of the figure. For a flexible chain (snapshots (i) to (iii)), the chain size decreases gradually as C_s increases up to C_s^*; the chain undergoes a continuous coil-to-globule transition. The chain size then turns to increase slowly when $C_s > C_s^*$, indicating a swelling transition. C_s^* is found equal to 8×10^{-5}, the equivalence point. At this particular salt concentration, the added tetravalent counterions are in charge equivalence with the bare charge of the PE chain. We observed that the chain displays a disordered, globule structure at C_s^*. For a semiflexible chain (snapshots (iv) to (vi)), two sharp transitions take place at low and at high salt concentrations, respectively. They are, in turn, the coil-to-globule and the globule-to-coil transitions. It

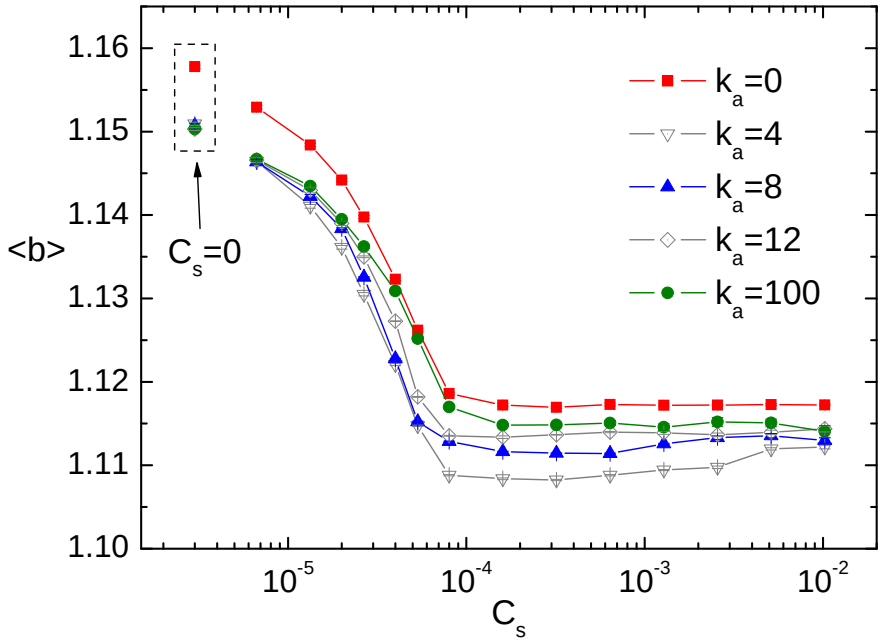

FIG. 2: $\langle b \rangle$ as a function of C_s for different chain stiffness k_a. The values of k_a are indicated in the figure. The data for $C_s = 0$ are also plotted in the dashed box on the left-top side of the figure.

has been shown that these two transitions occur in a discrete manner [43], in contrast to the continuous transitions happened for a flexible chain. In the region between the two salt concentrations, the chain is in a collapsed state and exhibits a compact ordered structure, such as a toroidal structure or a folded-chain structure. Outside the salt region, the chain structure becomes extended. This kind of phenomena is called "reentrant condensation" and has attracted much attention in the study of DNA condensation [6, 7]. For the case of a rigid chain (snapshot (vii)), the chain is so stiff that it cannot be folded by the condensed multivalent counterions. The chain stays elongated, no matter how many salts are added in the solution.

In addition to the chain size and morphology, which are global properties of chain in solutions, we studied also local properties such as the average bond length. This information tells us how the bond length changes in different conditions, which is directly related to the line charge density of a PE chain, and is important, later on, in the comparison with the Manning condensation theory. The average bond length $\langle b \rangle$ as a function of C_s is shown in Fig. 2. The chains of different stiffness show similar variational behavior. $\langle b \rangle$ decreases with increasing C_s when $C_s \leq C_s^*$. It then stays basically at a constant for $C_s > C_s^*$. The maximum reduction of $\langle b \rangle$ is less than 4%. We remark that this decreasing in $\langle b \rangle$ is

a result of the condensation of multivalent counterions on a PE chain, which form triplets with monomers (as we will see in Section III F) and hence pull closer the distance between two neighboring monomers via the Coulomb interaction. In the region $C_s > C_s^*$, although the chains are charge overcompensated (cf. Fig. 6), the extra number of the condensed ions cannot pull closer the monomer-monomer distance anymore due to the excluded volume effect. $\langle b \rangle$ is thus saturated at a constant value. Combining with the information that R_h increases when $C_s > C_s^*$, we know that the bond length is not responsible for the global chain reexpansion in this region.

B. Ion distribution in chain radial direction

After knowing the morphology of PEs in different salt and chain stiffness conditions, we study now different kinds of ion distributions and their relation with the chain morphology. We focus firstly on the ion distribution in chain radial direction. A tube region around a chain is defined as the union of spheres of radius r_t, centered at each monomer center. The average number of ions inside this tube region is calculated for each ion species. By varying r_t, we are able to investigate the integrated ion distribution $N_t(r_t)$ around the chain radially. The results for monovalent counterions, tetravalent counterions, and coions are shown in Fig. 3.

Fig. 3(a) shows typical ion distributions in the low salt region, $C_s < C_s^*$. Manning condensation theory [12, 45] states that in salt-free solutions, if the value of ξ, defined as the ratio of the Bjerrum length λ_B to the charge distance on the chain backbone $\langle b \rangle$, is greater than unity, the condensed counterions will neutralize the fraction $1 - \xi^{-1}$ of charge on the rigid PE chain. According to this theory, there should be about 61.7% of the monovalent counterions, or equivalently 30 monovalent counterions, condensing on the PE chain at $C_s = 0.0$ in our simulation condition ($\lambda_B = 3$ and $\langle b \rangle \simeq 1.15$; thus, $\xi = 2.61$). In this figure, we see only about 20 monovalent counterions condensing on the chain (inside the tube region with $r_t = \lambda_B = 3$). This is because the tetravalent counterions added in the solution compete with the monovalent ones and replace part of the condensed monovalent counterions on the chain. Therefore, the number of condensed monovalent counterions is smaller than that in the sat-free solution. Moreover, we observed that when $r_t > 3$, the integrated number $N_t(r_t)$ for tetravalent counterions is a constant. This result indicates that nearly all the tetravalent

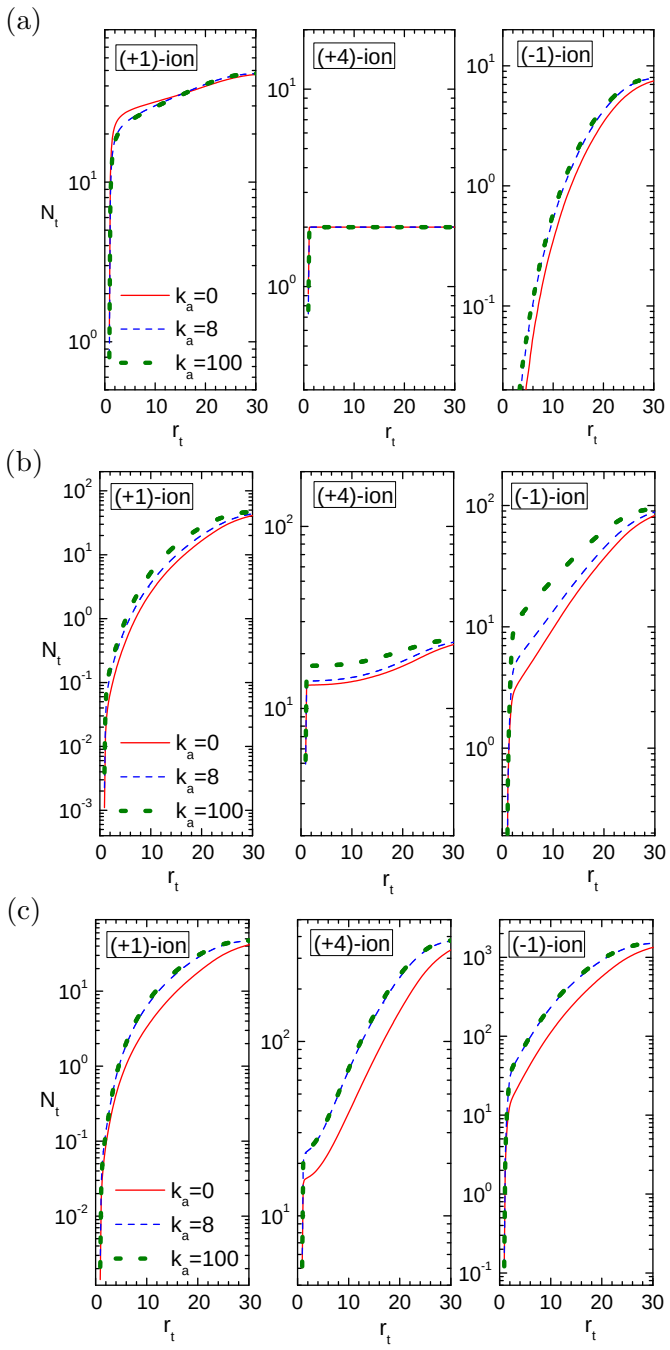

FIG. 3: Integrated number of ions $N_t(r_t)$ for monovalent counterions ((+1)-ion), tetravalent counterions ((+4)-ion), and coions ((-1)-ion), around a chain at $C_s = 1.33 \times 10^{-5}$ (a), 1.6×10^{-4} (b), and 2.56×10^{-3} (c). The values of chain stiffness k_a are indicated in the figure.

counterions condense on the chain in this low salt region. Fig. 3, panels (b) and (c), show typical ion distributions in the middle ($C_s \sim C_s^*$) and in the high ($C_s > C_s^*$) salt regions. We saw that $N_t(r_t)$ for monovalent counterions is almost zero inside the tube $r_t = 3$. Thus, the condensed ions are now tetravalent in majority. For tetravalent counterions, $N_t(r_t)$ is

no more a constant when $r_t > 3$. There are hence non-condensed tetravalent counterions presented in the bulk solution.

Form the above three figures, we can see that the ion distributions depend strongly on the chain morphology. For example, at low C_s (Fig. 3(a)), the morphology of the flexible chain ($k_a = 0$) is an extended coil, whereas the semiflexible chain ($k_a = 8$) is elongated and rodlike, resembling the rigid chain ($k_a = 100$). Therefore, the ion distribution curves are nearly identical for the two cases $k_a = 8$ and $k_a = 100$. Similar results are found at high C_s (Fig. 3(c)) where the chains reenter into the solution. In that case, the reentered semiflexible chains is as extended as a rod, different from the coil structure of a flexible chain. As a consequence, the $N_t(r_t)$ curve is distinguishable to that for the flexible chain, but similar to the rigid chain. In the mid-salt region (Fig. 3(b)), the flexible and the semiflexible chains are collapsed, due to the condensation of tetravalent counterions, but the collapsed chain structures are different: a disordered globule structure for the former chains and an ordered structure for the latter. $N_t(r_t)$ curves are therefore non-identical for the three chain stiffness.

The ion distributions for the semiflexible chain ($k_a = 8$) were further investigated in detail in the middle salt region because in this region the chains can collapse into one of the two typical structures: toroid and hairpin structures. We observed that (in Fig. 4(a)) toroidal chains and hairpin chains show similar ion distributions. The reason is that the condensed tetravalent counterions bridge between chain segments in these two cases to force the chains to form toroid or hairpin. Consequently, the ion distributions look similar along the viewpoint of the chain radial direction. Moreover, when the salt concentration is close to the globule-to-coil transition, our previous study showed that the semiflexible chains can alter between three structures: the toroid, the hairpin and the extended-rod structures [43]. Since the toroid and the hairpin structures give a similar distribution of ions around a chain, it is relevant to verify whether or not the $N_t(r_t)$ curve for the extended-rod chain structure is also distinguishable to the collapsed chain structures (toroid and hairpin). The results are presented in Fig. 4(b) and significant differences are observed. We found that the more the chain morphology is opened or extended, the larger the $N_t(r_t)$ will be. This is because more space is available for ions to condense or to approach to a chain when the chain has an opened structure. For example, in Fig. 3(b), the elongated chains ($k_a = 100$) have a larger value of $N_t(r_t)$ than the toroid or hairpin chains ($k_a = 8$), and than the chains collapsed into disordered globule structure ($k_a = 0$). Similar results have been also observed

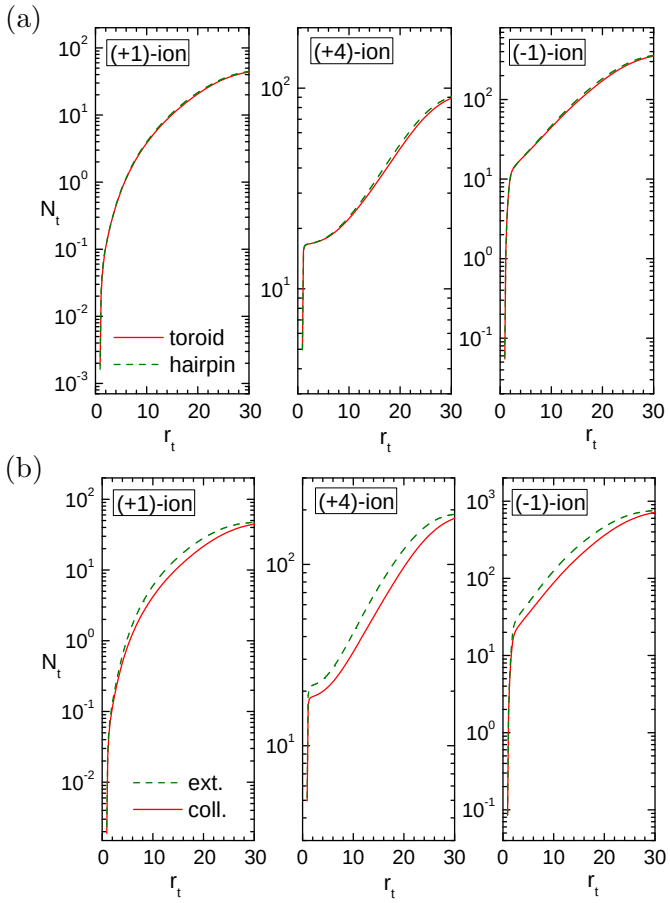

FIG. 4: $N_t(r_t)$ for the semiflexible chains ($k_a = 8$) (a) at $C_s = 6.4 \times 10^{-4}$ where the chains are of toroid and of hairpin structures, (b) at $C_s = 1.28 \times 10^{-3}$ where the chains are in an extended (ext.) state and in a collapsed (coll.) state.

in Figs. 3(a), 3(c) and 4(b). The above evidences show that ion distributions around a chain are determined by chain morphology, while chain morphology depends on chain stiffness and salt concentration.

C. Charge distribution in chain radial direction

Using the information obtained in the previous section, by summing up all of the charges inside a tube region around a chain, we studied the integrated charge distribution $Q_t(r_t)$. The results are shown in Fig. 5 for the flexible, the semiflexible, and the rigid chains, over a broad range of salt concentration. We observed that when $C_s < C_s^* = 8 \times 10^{-5}$, $Q_t(r_t)$ is a monotonic increasing function of r_t with the value increasing from -48, the bare charge of chain, to 0, due to the electro-neutrality of the system. In this salt region, the value of

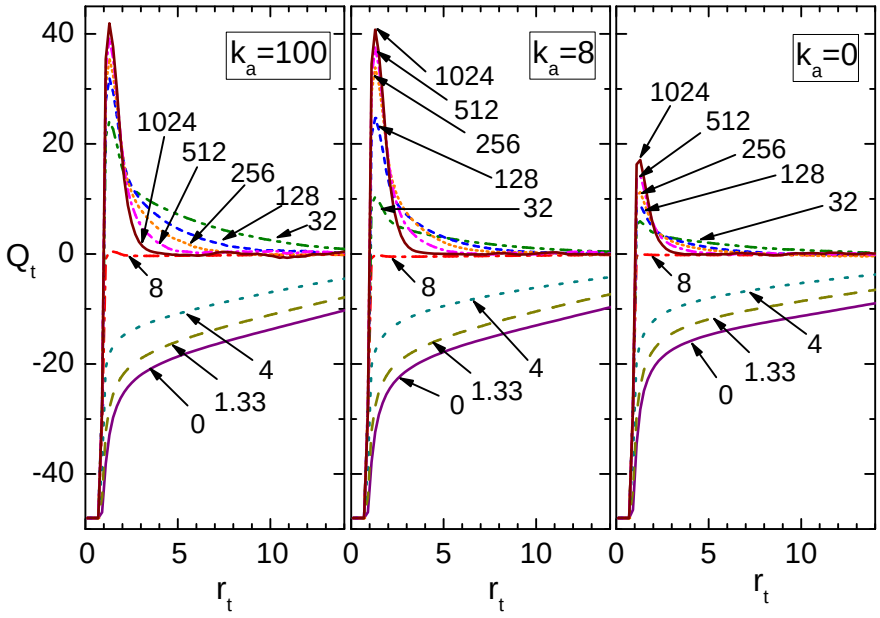

FIG. 5: $Q_t(r_t)$ for the rigid ($k_a = 100$), the semiflexible ($k_a = 8$), and the flexible ($k_a = 0$) chains. The number ($\times 10^{-5}$) near each curve is the salt concentration C_s.

$Q_t(r_t)$ increases with C_s at a given r_t. When the system is at the equivalence point C_s^*, the curve $Q_t(r_t)$ turns out to be zero outside the region of chain excluded volume ($r_t > 1$). This result tells us an important information that the condensed ions completely neutralize the chains such that the total charge inside the tube region is zero. When $C_s > C_s^*$, $Q_t(r_t)$ starts to show a positive peak near the chain surface at $r_t \simeq 1.2$. The peak decays rapidly to zero. The result indicates the occurrence of charge overcompensation; that is, there is an excessive number of tetravalent counterions condensing on the chain surface than needed to neutralize it. A charge overshooting thus takes place. The higher the salt concentration, the more pronounced the peak will be. Moreover, we found that the rigid and the semiflexible chains are more overcharged than the flexible chain. This is because the opened chain structure provides larger space to condense multivalent counterions, leading to a more pronounced $Q_t(r_t)$ peak.

D. Ion condensation on a chain and the effective chain charge

In the last two sections, the integrated ion and charge distributions were studied as a function of r_t. These figures contain detailed information at any given tube radius. Nonetheless, in a general discussion, people usually concern about the number of the condensed ions

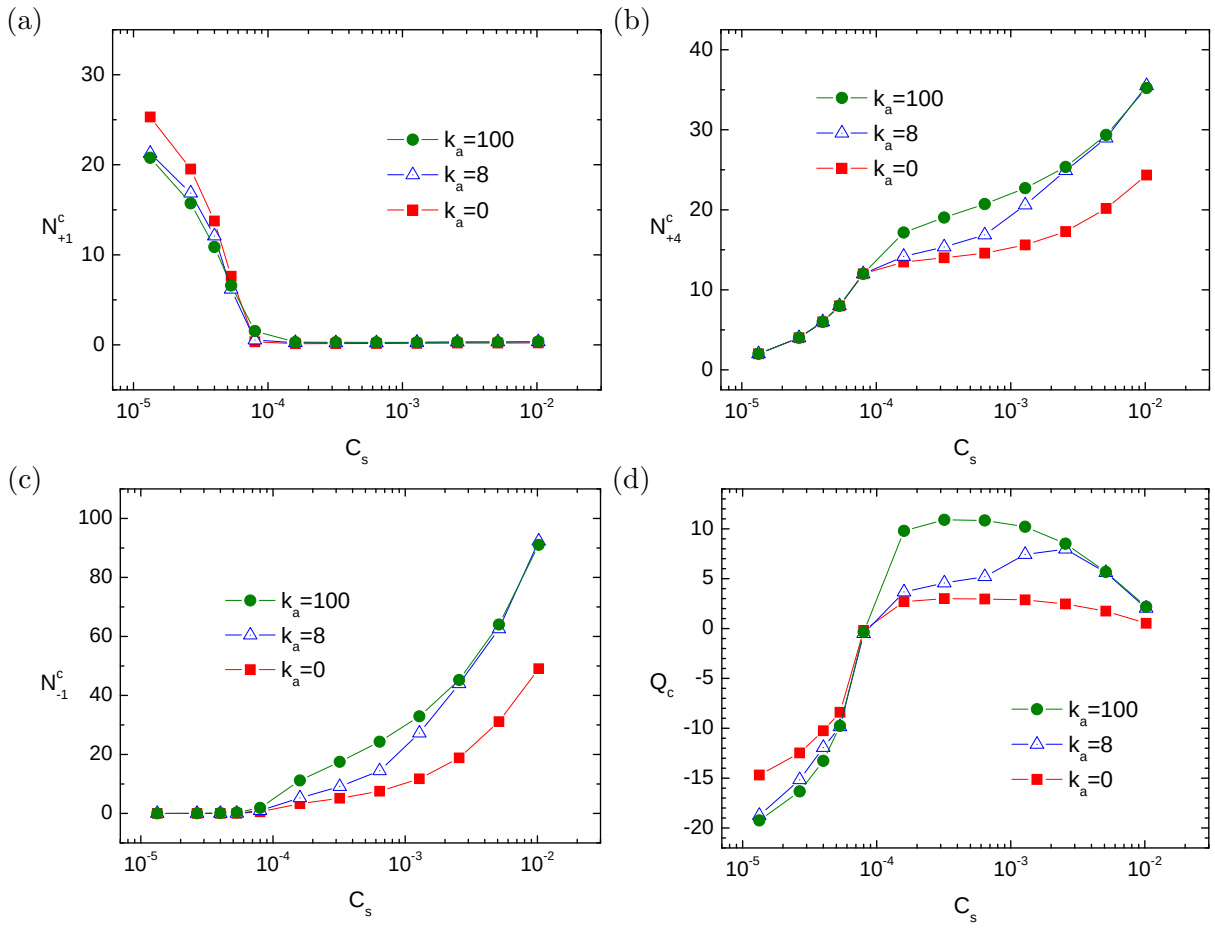

FIG. 6: (a) N^c_{+1}, (b) N^c_{+4}, (c) N^c_{-1}, and (d) Q_c as a function of C_s. The values of chain stiffness k_a are indicated in the figures.

on a chain and pay more attention on the effective chain charge resulting from the ion condensation. To study these topics, one needs to know firstly the region of ion condensation. However, there exists no clear boundary to separate the condensation region from the non-condensation one. We remark that the condensation region is simply a concept, which can be only qualitatively described. In this study, we define the condensation region to be the tube region around a chain with r_t equal to the Bjerrum length λ_B (= 3). This definition is based upon the Manning condensation theory [12, 45]. The results for the three different chain stiffness are shown in Fig. 6, panels (a)–(d), where the numbers of the condensed monovalent counterions (N^c_{+1}), the condensed tetravalent counterions (N^c_{+4}), and the condensed coions (N^c_{-1}), together with the effective charge of chain inside the condensation region (Q_c), are presented as a function of salt concentration.

Focus firstly on the lowest salt concentration $C_s = 1.33 \times 10^{-5}$ in the figures. At this

C_s, 2 tetravalent counterions and 8 monovalent coions are added into the simulation box (refer to Table I). The results, $N^c_{+4} = 2$ and $N^c_{-1} = 0$, show that the tetravalent counterions entirely condense on the chain whereas the coions stay all in the bulk solution. Manning condensation theory predicts that the condensation of counterions on a rigid chain in a salt-free solution should result in an effective chain charge density equal to $1/\lambda_B$ (in charge unit) [12, 45]. In our simulations, $N = 48$ monomers constitute a chain and the charge distance on a chain is $\langle b \rangle \simeq 1.15$ (see Fig. 2). There are hence $(1 - \langle b \rangle / \lambda_B)N = (1 - \xi^{-1})N$, about 30 monovalent counterions neutralizing the chain at $C_s = 0.0$, according to the theory. Since 2 condensed tetravalent counterions could repel 8 monovalent counterions originally condensed on the chain, back into the bulk solution, we expect a reduction of the number of the condensed monovalent counterion, N^c_{+1}, to a number of about 22. This is exactly what we observed in Fig. 6(a) for the rigid ($k_a = 100$) and the semiflexible ($k_a = 8$) chains. Please notice that N^c_{+1} for the flexible chain ($k_a = 0$) is larger than 22. It suggests a stronger ion condensation.

Focus next on the low salt region $C_s \leq C^*_s = 8 \times 10^{-5}$. We can see that N^c_{+4} increases with C_s. In fact, N^c_{+4} is equal to the number of tetravalent counterions added into the simulation box. It shows a full condensation of these ions on the chain. In this salt region, the N^c_{+4} curves overlap with each other, regardless of the chain stiffness. For condensed coions, we found $N^c_{-1} = 0$. It suggests that the chains repel the coions. This fact can be examined in Fig. 6(d) where the effective chain charge Q_c indeed takes a negative value (when $C_s \leq C^*_s$). Therefore, the coion condensation is unfavored because of the Coulomb repulsion. Concerning the condensation of monovalent counterions on a chain, we found that the number decreases with increasing C_s and hits the minimum value, zero, at $C_s = C^*_s$. At the same moment, Q_c increases and crosses eventually the zero point.

Focus thirdly on the high salt region $C_s > C^*_s$. We observed that N^c_{+4} continuously increases with C^*_s but splits into different curves, depending on the chain stiffness. These splitting curves are upper bounded by the curve coming from the rigid chain, while lower bounded by the one coming from the flexible chain. For the semiflexible chain, N^c_{+4} follows at beginning the lower-bounded curve and then transfers gradually to the upper-bounded curve. Once reexpanded in the solutions ($C_s > 3 \times 10^{-3}$), the chain looks similar to a rigid rod and the curve overlaps with the upper-bounded curve. Please notice that N^c_{+4} is larger than the number needed to neutralize the bare chain charge. Charge overcompensation

hence takes place and the chain charge turns to be positive. We note that in this salt region, the tetravalent counterions are not always condensed on the chain; in other words, fraction of them stay in the bulk solution. Since the chain charge is effectively positive, the coions can be attracted toward the chain but not the monovalent counterions. For this reason, N^c_{-1} starts to increase with C_s (see Fig. 6(c)) but N^c_{+1} stays at zero (see Fig. 6(b)). We observed that N^c_{-1} behaves similarly to N^c_{+4}, which split into curves depending on the chain stiffness. This behavior is directly associated to that of the N^c_{+4} because coion condensation necessitates the help of bridging by excessively condensed tetravalent counterions. For the effective chain charge, we did observe that Q_c becomes positive when $C_s > C^*_s$. Nevertheless, the Q_c curve does not trivially follow the N^c_{+4} curve. It shows convex-down behavior at some salt concentration. The decrease of Q_c tells us that the condensing rate for coions exceeds 4 times of that for tetravalent counterions beyond the salt concentration. Again, Q_c splits into different curves when $C_s > C^*_s$ with the upper bound being the case of the rigid chain and the lower bound being the case of the flexible chain. Q_c for the semiflexible chain deviates from the upper bound in the mid-salt regions because drastic change of chain conformation occurs in this region, very distinguishable to the morphology of the rigid chain. Finally, a trend was observed when C_s is very high: Q_c tends to zero, no matter of which stiffness the chain is. The charged chains are effectively neutralized.

The results obtained in this section demonstrate again that it is the chain morphology deciding the ion condensation and the effective chain charge. The chain stiffness plays a role, behind curtains, to determine the chain morphology at a given salt concentration.

E. Distribution of condensed ions in chain axial direction

In the previous three sections, we have investigated the ion distribution and condensation in the radial direction away from a chain axis. However, the pertinent information concerning the distribution in the perpendicular direction, *i.e.*, in the direction of the chain axis, is still missing. In order to fill up this gap of information, we investigate here how condensed ions distribute along a chain axis. The distribution is calculated by the following way. We firstly index the monomers sequentially, starting by 1, from one end of the chain to the other. We then assign each condensed ion (inside the condensation region $r_t = 3$) to a monomer, to which from the ion the distance is the shortest. The average numbers of the condensed ions

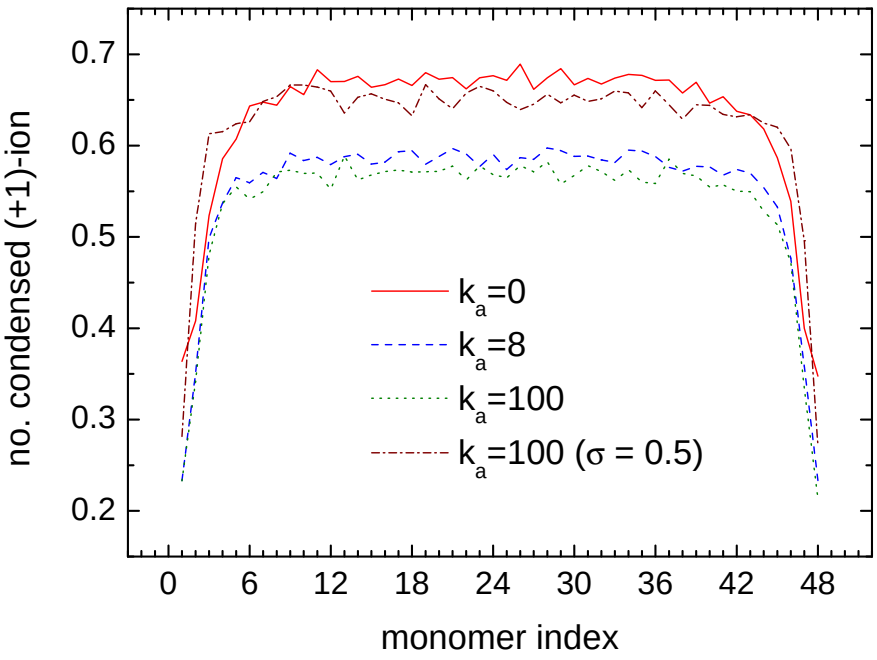

FIG. 7: Mean number of condensed monovalent counterions vs. monomer index in a salt-free solution for three chain stiffness, $k_a = 0$, 8 and 100. In order to show the importance of ion excluded volume, we plotted, in addition, the case of $k_a = 100$ with the ion size being reduced to half of the original one, marked by $\sigma = 0.5$.

assigned to every monomer are thirdly calculated for each ion species. The results give the ion distribution along the chain.

Fig. 7 shows the distribution of the condensed monovalent counterions in a salt free solution. Each curve denotes one chain stiffness. We observed that the distributions show plateau structure in the central part of the chains, while exhibiting a rapid decrease when the monomers approach to the two chain ends. It shows that the counterions are more likely to condense on the central part than on the two ends. When condensing onto the central part, a counterion is attracted by the monomers from both sides of the chain, while it is attracted only by one side of the chain if the condensation occurs near the chain ends. The Coulomb attraction is therefore stronger for the former case, and as a consequence, the condensed counterions are more numerous in the chain center. The results are in agreement with the works done by other groups [25, 29, 34]. Moreover, we found that the value at the plateau is higher for the flexible chain than for the rigid chain, which shows that monovalent counterions condense more strongly when the chain is flexible. We know that a flexible chain displays a zig-zagged structure when counterions condense onto it and becomes less

extensive compared to a semiflexible chain and a rigid chain [43]. Consequently, the line charge density on a flexible chain is effectively higher, which can lead to a stronger ion condensation. To examine it, we calculated the average angle $\langle\theta\rangle$ between two adjacent bonds for the three cases of chain stiffness, and the results are $\langle\theta\rangle = 121.8(5)^\circ$, $160.7(2)^\circ$, and $174.3(1)^\circ$ for the flexible ($k_a = 0$), the semiflexible ($k_a = 8$), and the rigid ($k_a = 100$) chains, respectively. The effective charge distance in the main direction of the zig-zagged chain axis thus can be estimated by $\langle b_{\rm eff}\rangle = \langle b\rangle \sin(\langle\theta\rangle/2)$. To adapt it for the chains with flexibility, We modify the Manning condensation theory by replacing the charge distance on the chains with the effective charge distance. The modified theory predicts a fraction of charge neutralization on the chains equal to $1-\langle b_{\rm eff}\rangle/\lambda_B$, which yields 0.665, 0.622, and 0.617 condensed monovalent counterions per monomer for the three studied stiffness, respectively. Our simulations show consistent trend of behavior with the theory. Nonetheless, the numbers are slightly smaller than the predictions. This is because the Manning theory was derived under the assumption of pointlike ions condensing onto an infinite cylindrical chain. Our modeling ions have excluded volume and the PE chain has finite chain length; both of the effects can decrease the number of the condensed ions. To verify it, identical simulations have been performed for the rigid chain ($k_a = 100$) except that the counterions were set to be half of the original ion size. The result is also plotted in Fig. 7 in dash-dotted curve (denoted by $\sigma = 0.5$) for comparison. We observed that the number of the condensed ions increases, which shows the importance of ion excluded volume on ion condensation. Here, the distance of closest approach between the monomer and the counterion is also a relevant parameter. The smaller the ion size, the closer the distance, and therefore, the stronger the condensation.

We next concentrate on the systems with added tetravalent salt. Since the tetravalent counterions play a crucial role in determination of chain morphology by substituting the condensed monovalent counterions on a chain, we study here how the condensed tetravalent counterions distribute on a chain.

Fig. 8(a) shows such distribution on the rigid chain ($k_a = 100$). At the low salt concentration $C_s = 2.67 \times 10^{-5}$, the ions distribute uniformly on the chain backbone except near the chain ends. The distribution profile looks similarly to that for monovalent counterions in salt-free solution. This is because many monovalent counterions still condense on the chain (cf. Fig. 6(a)) and collide with the condensed tetravalent counterions. The

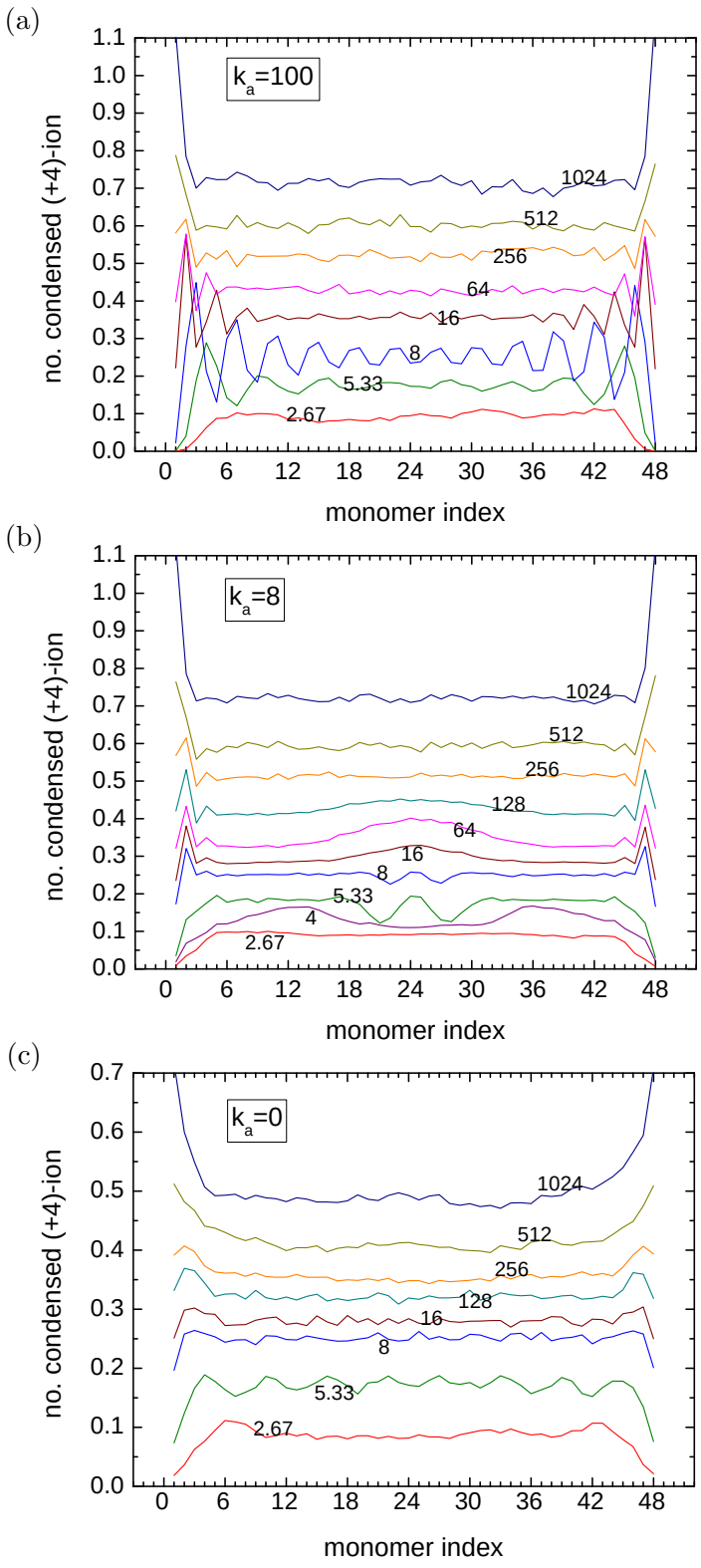

FIG. 8: Mean number of condensed tetravalent counterions vs. monomer index for (a) the rigid chain, (b) the semiflexible chain, and (c) the flexible chain. Each curve denotes one distribution at a salt concentration C_s. The value of $C_s \times 10^5$ can be read near the corresponding curve.

condensed tetravalent ions thus diffuse on the chain, resulting in a uniform distribution. As C_s increases, the condensation of tetravalent counterions ensures a rapid decrease of the number of the condensed monovalent counterions. Eventually, the tetravalent ions become the majority on the chain and the strong electrostatic repulsion between them induces the localization of these ions at some specific positions along the one-dimensional chain. This is why at $C_s = 5.33 \times 10^{-5}$ and 8.0×10^{-5}, several peaks appear on the distribution profile. The number of the peaks corresponds to the number of the tetravalent ions condensed on the chain, which is exactly the amount of these ions added in the simulation box (cf. Table I). When C_s is increased over the equivalence point $C_s^*(= 8.0 \times 10^{-5})$, the number of the condensed tetravalent counterions exceeds the one needed to neutralize the chain backbone charge. Charge overcompensation takes place. The ion localization is now disturbed by these extra ions. The disturbing shows its effect starting from the central part of the chain and propagating to the chain ends with increasing the salt concentration. Finally, the distribution becomes uniform again. We found that, different to the cases at low salt concentrations, the tetravalent ions favor to condense on the chain ends when C_s is high. This is because near the chain ends, there are more spaces available to accommodate these over-crowded ions.

Fig. 8(b) shows the distribution on the semiflexible chain ($k_a = 8$). When $C_s < 4 \times 10^{-5}$ or $C_s > 1.28 \times 10^{-3}$, the PE chain displays an extended structure. Similar to the rigid chain, the condensed tetravalent ions distribute uniformly on the chain backbone. In between the salt concentrations, the chain forms ordered collapsed structure and the distribution displays some specific profile. For example, at $C_s = 4 \times 10^{-5}$, the distribution shows a symmetric profile with two humps. This profile results from a particular hairpin structure in which the length of the two branches of the hairpin is not equal (cf. snapshots in Fig. 9). Each hump in the distribution reflects the drastic change of chain geometry at an eccentric bending point of the hairpin. We note that the appearance of the two humps do not mean two bendings in one hairpin. It is a result of ensemble average in which the probability of the bending point close to one of the two chain ends is equal when the system is in equilibrium. Therefore, the distribution is a symmetric function with respect to the middle point. At $C_s = 5.33 \times 10^{-5}$ and 8×10^{-5}, the number of the condensed ions is sufficiently numerous to bind the chain, against the chain stiffness, to form a hairpin with two equal branches (cf. Fig. 9). A condensed counterion is localized at the bending point, which results in the

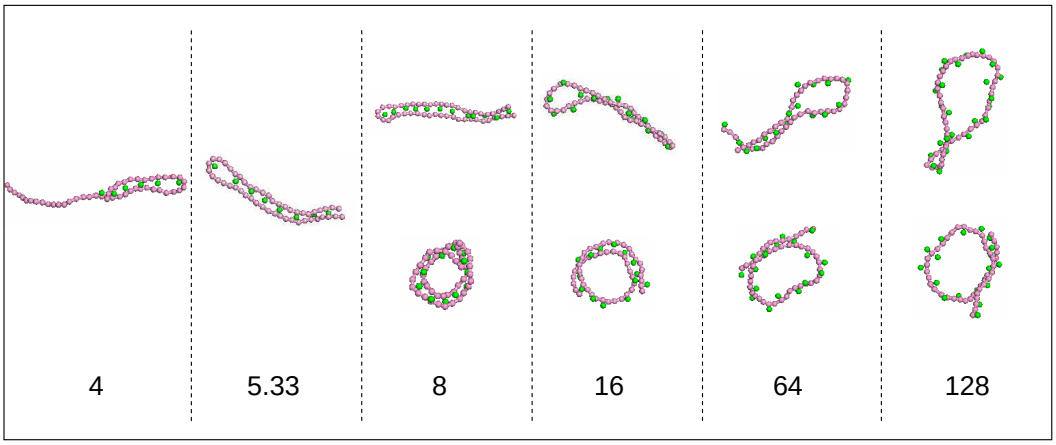

FIG. 9: Snapshots of typical morphologies of the semiflexible chain ($k_a = 8$). The numbers below the pictures are the salt concentrations ($\times 10^5$).

peak at the middle point of the chain. For $C_s > 8 \times 10^{-5}$, the number of the condensed tetravalent ions is excess. A loop is formed near the hairpin head in order to create more room to accommodate these extra ions. The chain morphology thus looks similar to a tennis racquet. The more the excess number of the ions, the larger the loop will be formed and the distribution shows a broader and higher hump near the middle of the chain. We remark that when $8 \leq C_s \times 10^5 \leq 128$, toroid is also a favored structure of the chain. The ion distribution on toroidal structure is similar to the one on a hairpin (or a racquet), which displays a hump in the middle. To help readers to obtain the whole pictures of the system in mind, we present in Fig. 9 typical snapshots of the semiflexible chain together with the condensed tetravalent counterions in the middle range of salt concentration.

Figure 8(c) shows the distribution on the flexible PE ($k_a = 0$). We have learned that the flexible chain is collapsed into a disordered structure when the salt concentration is intermediate. The condensed tetravalent ions cannot be localized at some specific positions of the chain. The distribution hence shows a uniform distribution. By comparing Fig. 8(a), (b) and (c), we noticed that the number of the condensed tetravalent counterions is less numerous for the flexible chain than for the semiflexible and the rigid chains when $C_s > C_s^*$. The reason is that the flexible chain occupies a smaller volume space compared to the other two chain stiffness (cf. Fig. 1). Consequently, smaller room is available to accommodate the strongly-repelled tetravalent ions, leading to fewer condensed tetravalent counterions. It is worth noticing that in the condensation of the monovalent counterions at $C_s = 0$ (cf.

Fig. 7), the number of condensed monovalent counterions is more numerous for the flexible chain, which shows an opposite trend to this case.

F. Radial distribution function between monomers and tetravalent counterions

In addition to the ion distributions in the radial and in the axial directions discussed in the above sections, we study also the radial distribution function $g_{m,+4}(r)$ between monomers and tetravalent counterions. $g_{m,+4}(r)$ is defined as the averaged density function $\langle \rho_{m,+4}(r) \rangle$ of the tetravalent counterions around a monomer dividing the mean density of the tetravalent counterions in the whole system, C_s. It is a correlation function, which provides the information of organization of the tetravalent counterions surrounding an individual monomer. The results at different C_s are presented in Fig. 10 for the three chain stiffness, $k_a = 0$, 8, and 100.

Fig. 10(a) shows $g_{m,+4}(r)$ for the rigid chain ($k_a = 100$). The distribution functions show a series of peaks located subsequently at r = 1.0, 1.8, 2.9, 3.9, 5.0, ... Since the chain conformation is a straight line, the results indicate that the condensed tetravalent counterions sit on the clefts between two adjacent monomers and form triplets with monomers, as sketched in the cartoon picture (inside the figure), because the peak positions match well the distances calculated from the picture. Similar triplet formation has been reported by other group using monovalent counterions, instead [46]. When $C_s \leq C_s^*$, the distribution functions overlap with each other. This is because nearly all of the tetravalent counterions condense on the chain in this salt region. As a result, the correlations between monomers and tetravalent counterions are identical. When $C_s > C_s^*$, the curves move downward with increasing C_s. The correlation decreases, owing to the increase of the non-condensed tetravalent counterions presented in the bulk solutions.

$g_{m,+4}(r)$ for the semiflexible chain ($k_a = 8$) displays subsequent peaks too, as shown in Fig. 10(b). However, these peaks are broader and less pronounced, in comparison with the previous case, because thermal fluctuations can take effect on chain conformation for this chain stiffness. Since the chain collapses in the intermediate salt region, the size of the chain reduces, leading to a faster decay of $g_{m,+4}(r)$ against r.

$g_{m,+4}(r)$ for the flexible chain ($k_a = 0$) shows only one peak at $r = 1$ (see Fig. 10(c)). This peak marks the close contact of the counterions with a monomer. It is more pronounced

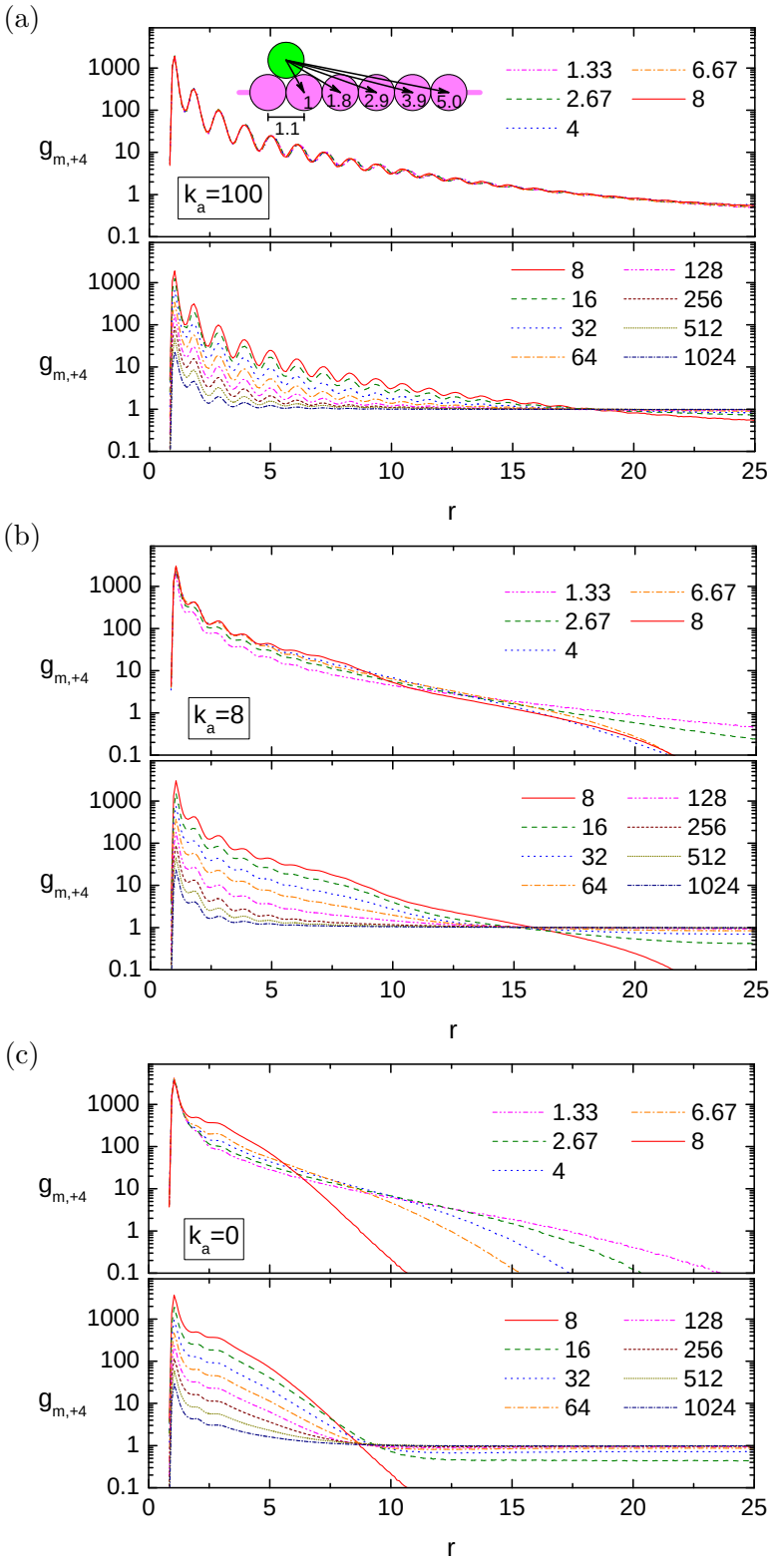

FIG. 10: $g_{m,+4}(r)$ for (a) the rigid chain, (b) the semiflexible chain, and (c) the flexible chain at different C_s. The value of $C_s \times 10^5$ is indicated in the figures.

than the first peak for the semiflexible and the rigid chains, suggesting a stronger correlation. Following the peak, a broad shoulder appears on the right-hand side. The shoulder narrows down to a finite region when the salt concentration is increased from 1.33×10^{-5} to 8×10^{-5}. This behavior reflects two facts: (1) the nature of random arrangement of tetravalent counterions surrounding a monomer when the chain is flexible, (2) the reduction of chain size in the intermediate salt region.

IV. CONCLUSIONS

Using Langevin dynamics simulations, we have studied ion and charge distributions in PE solutions from various points of view. The discussed topics focused on the effects of the two parameters: the salt concentration and the chain stiffness. The salt concentration ran over a wide range of value in which the reentrant condensation takes place, and the chain stiffness covers the three types of behavior discussed in Section III A. The results showed that the ion and the charge distributions depend strongly on the morphology of a chain, while the morphology is determined by both of the two parameters. When the salt concentration is low and cannot induce collapse of chain, the ion distribution shows similar profile for flexible, semiflexible and rigid chains, because these chains all display extended structures. In the middle salt region, the chain charge is nearly neutralized by the condensed multivalent counterions. The chains show drastic conformational change. The flexible chains are collapsed into disordered globule structures whereas the semiflexible chains are collapsed into ordered structures such as toroid and hairpin. For the rigid chains, the chain conformation remains rodlike. Since the chain morphologies are different for these three kinds of chain stiffness, the ion distributions show significant difference. A general rule is that the larger the space that a chain structure occupies, the more the ions can condense on a chain. Therefore, the number of the condensed ions and the effective chain charge for the semiflexible chains are upper- and lower-bounded by those curves for the flexible and the rigid chains, respectively. In the high-salt region, the condensed multivalent counterions overcompensate the chain charge on the chain surface. The flexible and the semiflexible chains reexpand in the solutions. The latter chain displays a rodlike structure, more extended than the former one which displays a coil structure. Therefore, the semiflexible and the rigid chains show similar ion distributions, distinguishable to the flexible chain. The study

of the condensed ion distribution in the chain axial direction tells us other information. At low or at high salt concentrations, the condensed ions distribute uniformly on the chain backbone (because the chain is not collapsed), whereas at intermediate salt concentrations, the distribution showed specific profile which has direct connection with the structure of the collapsed chains. Finally, in the study of the radial distribution function, we demonstrated that a condensed multivalent counterion favors to form a triplet with two adjacent monomers. Consequently, the radial distribution of multivalent counterions shows a series of peaks away from a monomer.

Before the closure of this paper, we describe more about how flexible chains and semiflexible chains get reexpanded in a high-salt region. According to Fig. 6, the number of the condensed multivalent counterions increases monotonically when the salt concentration is increased. We know that flexible chains and semiflexible chains are both collapsed and charge-neutralized at the equivalence point C_s^*. Further condensing the multivalent counterions leads to the arising of the repulsive forces, including the Coulomb repulsion and the excluded volume interaction, in the interior of the collapsed chain structures. The collapsed chains are therefore getting looser and becomes more and more unstable. For a flexible chain, the chain unfolds gradually into a coil structure. Similar results have been reported recently in the simulation study of other flexible charged systems, such as dendrimers [47] and spherical polyelectrolyte brushes [48]. In these studies, the dendrimers and the PE brushes were collapsed by multivalent salt and oppositely charged linear PEs, respectively. When the concentration of these condensing agents is higher than the equivalence point, the collapsed structures reswell due to the excluded volume and the repulsive interactions of the condensing agents excessively adsorbed on the systems. The reswelling goes in a continuous way [43]. For a semiflexible chain, there exists, in addition, a restoring force, owing to the intrinsic chain stiffness, which plays a crucial role in the chain reexpansion. The binding of chain segments in a collapsed chain structure decreases when the excess number of the condensed counterions increases. Once the restoring force can overcome the binding force, the chain reexpands in a sudden and drastic way. A first-order transition takes place [43]. The detailed information provided in this study gives valuable insight to the problem of DNA condensation and can help researchers to develop new models to explain these phenomena more quantitatively.

V. ACKNOWLEDGMENTS

This material is based upon work supported by the National Science Council, the Republic of China, under Contract No. NSC 95-2112-M-007-025-MY2 and NSC 97-2112-M-007-007-MY3. Computing resources are supported by the National Center for High-performance Computing under the project "Taiwan Knowledge Innovation National Grid".

---

[1] W. M. Gelbart, R. F. Bruinsma, P. A. Pincus, and V. A. Parsegian, Physics Today **53**, 38 (2000).

[2] A. Y. Grosberg, T. T. Nguyen, and B. I. Shklovskii, Rev. Mod. Phys. **74**, 329 (2002).

[3] Y. Levin, Rep. Prog. Phys **65**, 1577 (2002).

[4] G. C. Wong, Curr. Opin. Colloid Interface Sci. **11**, 310 (2006).

[5] T. Iwaki, T. Saito, and K. Yoshikawa, Colloid Surf. B-Biointerfaces **56**, 126 (2007).

[6] V. A. Bloomfield, Curr. Opin. Struct. Biol. **6**, 334 (1996).

[7] V. A. Bloomfield, Biopolymers **44**, 269 (1997).

[8] R. Messina, J. Phys.:Condens. Matter **21**, 113102 (2009).

[9] M. Olvera de la Cruz, L. Belloni, M. Delsanti, J. P. Dalbiez, O. Spalla, and M. Drifford, J. Chem. Phys. **103**, 5781 (1995).

[10] J. Pelta, F. Livolant, and J.-L. Sikorav, J. Biol. Chem. **271**, 5656 (1996).

[11] E. Raspaud, M. Olvera de la Cruz, J.-L. Sikorav, and F. Livolant, Biophys. J. **74**, 381 (1998).

[12] F. Oosawa, *Polyelectrolytes* (Marcel Dekker, 1971).

[13] I. Rouzina and V. A. Bloomfield, J. Phys. Chem. **100**, 9977 (1996).

[14] F. J. Solis and M. Olvera de la Cruz, J. Chem. Phys. **112**, 2030 (2000).

[15] F. J. Solis and M. Olvera de la Cruz, Eur. Phys. J. E **4**, 143 (2001).

[16] F. J. Solis, J. Chem. Phys. **117**, 9009 (2002).

[17] T. T. Nguyen, I. Rouzina, and B. I. Shklovskii, J. Chem. Phys. **112**, 2562 (2000).

[18] M. A. Young, B. Jayaram, and D. Beveridge, J. Am. Chem. Soc. **119**, 59 (1997).

[19] M. Feig and B. M. Pettitt, Biopolymers **48**, 199 (1998).

[20] S. Y. Ponomarev, K. M. Thayer, and D. L. Beveridge, Proc. Natl. Acad. Sci. USA **101**, 14771 (2004).

[21] J. L. abascal and J. C. G. Montoro, J. Chem. Phys. **114**, 4277 (2001).

[22] J. L. F. abascal, M. Domercq, and J. C. G. Montoro, J. Phys. Chem. B **110**, 25080 (2006).

[23] E. Allahyarov, H. Löwen, and G. Gompper, Phys. Rev. E **68**, 061903 (2003).

[24] E. Allahyarov, H. Löwen, and G. Gompper, Europhys. Lett. **68**, 894 (2004).

[25] S. Liu and M. Muthukumar, J. Chem. Phys. **116**, 9975 (2002).

[26] S. Liu, K. Ghosh, and M. Muthukumar, J. Chem. Phys. **119**, 1813 (2003).

[27] Z. Ou and M. Muthukumar, J. Chem. Phys. **123**, 074905 (2005).

[28] J. M. G. Sarraguça, M. Skepo, A. A. C. C. Pais, and P. Linse, J. Chem. Phys. **119**, 12621 (2003).

[29] J. M. G. Sarraguça and A. A. C. C. Pais, Phys. Chem. Chem. Phys. **8**, 4233 (2006).

[30] J. Kłos and T. Pakula, J. Chem. Phys. **122**, 134908 (2005).

[31] P.-Y. Hsiao, J. Chem. Phys. **124**, 044904 (2006).

[32] P.-Y. Hsiao, Macromolecules **39**, 7125 (2006).

[33] P.-Y. Hsiao and E. Luijten, Phys. Rev. Lett. **97**, 148301 (2006).

[34] H. J. Limbach and C. Holm, J. Chem. Phys. **114**, 9674 (2001).

[35] P. G. Arscott, A.-Z. Li, and V. A. Bloomfield, Biopolymers **30**, 619 (1990).

[36] G. E. Plum, P. G. Arscott, and V. A. Bloomfield, Biopolymers **30**, 631 (1990).

[37] G. Maurstad, S. Danielsen, and B. T. Stokke, J. Phys. Chem. B **107**, 8172 (2003).

[38] I. M. Lifshitz, A. Y. Grosberg, and A. R. Khokhlov, Rev. Mod. Phys. **50**, 683 (1978).

[39] C. B. Post and B. H. Zimm, Biopolymers **21**, 2123 (1982).

[40] K. Ghosh, G. A. Carri, and M. Muthukumar, J. Chem. Phys. **116**, 5299 (2002).

[41] K. Yoshikawa and Y. Matsuzawa, Physica D **84**, 220 (1995).

[42] K. Yoshikawa, M. Takahashi, V. V. Vasilevskaya, and A. R. Khokhlov, Phys. Rev. Lett. **76**, 3029 (1996).

[43] Y.-F. Wei and P.-Y. Hsiao, J. Chem. Phys. **127**, 064901 (2007).

[44] G. R. Strobl, *The physics of polymers : concepts for understanding their structures and behavior* (Springer, Berlin, 1997), 2nd ed.

[45] G. S. Manning, J. Chem. Phys. **51**, 924 (1969).

[46] T. S. Lo, B. Khusid, and J. Koplik, Phys. Rev. Lett. **100**, 128301 (2008).

[47] W.-D Tian, and Y.-Q. Ma, J. Phys. Chem. B **113**, 13161 (2009).

[48] R. Ni, D. P. Cao, W. C. Wang, and A. Jusufi, Macromolecules **41**, 5477 (2008).